

Fully Lagrangian Approach of Three-Phase Systems for Debris Bed Formation (Part II: Effect of Sphericity)

YoungWoo Son, InSoo Seo, Cheol-O Ahn*
Metariver Technology Co., Ltd., C-716, Moonjeong-SK-VI, 128,
Beobwon-ro, Songpa-gu, Seoul, 05854, Republic of Korea
*Corresponding author: coahn@metariver.kr

***Keywords** : DAVINCI experiment, three-phase flow, particle sphericity, drag coefficient, terminal velocity

1. Introduction

In case of a severe accident in a light water reactor, the breakup of the melt in water forms a porous debris layer on the bottom of the reactor cavity, and the characteristics of the debris layer are important for the adequate assessment of the coolability of the corium. [1][2][3][4]

To investigate the internal structure of the debris layer and the effect of the bubble generated by decay heat, Kim et al. [1][2] conducted an experimental study using the DAVINCI (Debris Bed Research Apparatus for Validation of the Bubble-Induced Natural Convection Effect Issue) test facility. They studied the structure of the debris layer obtained by injecting air bubbles from the bottom and dropping particles of various sizes into the water tank. In this experiment, the particle column formed by falling particles and the bubble column formed by air injection from the bottom each cause opposite flow and collide, resulting in very complex behavior and ultimately scattering the particles to the bottom. A complex flow field is formed by many bubbles generated by air injection, and it changes the settling path of the settling particles, affecting the formation of the debris bed. Therefore, to accurately predict the shape of the debris bed, it is important to consider the effect of the flow induced by bubbles as well as the behavior of particles of various shapes and sizes.

Since our simulation results using coupled MPS [4]-DEM-DBM [5] based on a fully Lagrangian approach with unresolved method were quantitatively compared with the DAVINCI experiments in the paper Part I of the same title, in this study we investigated the mass distribution of particles settling on the bottom according to the sphericity of the particles under the same conditions.

2. DAVINCI experiment

DAVINCI consists of three major parts: a particle injection system, a test pool, and a PCP module that equips an air injection system. The particle injection system is composed of a funnel and funnel rack to isolate the particle feed from the vibration of the convection flow in the pool. The particles were released by gravity after removing a rubber plug from the nozzle.

The test pool was fabricated from a transparent acrylic cylinder to allow visualization. Vapor generation from the hot debris bed was simulated with 32 air chambers in a predetermined air flow rate distribution. [1][2]

Particle sampling catchers were prepared to investigate the local characteristics of the internal structure of debris beds. A stainless steel mesh with an aperture of 0.1 mm was attached to the bottom of the particle sampling catchers to collect all of the settled particles while allowing air bubble penetration. [2]

The particles were made of stainless steel 304, and the density was measured to be about 8,000 kg/m³. The test SG used single-size particles and the test MT2 used five different particle sizes. The mass fraction of particles in the test condition was designed to simulate corium debris particles from the breakup and fragmentation of the melt jet, using the particle size distribution model of Moriyama et al. [2]

3. Numerical method

For more details on the numerical method, see Part I of the paper of the same title.

4. Numerical analysis

Fig. 1 (a) shows the terminal rising velocity corresponding to the bubble condition presented in the DAVINCI experiment by Kim et al. [1][2], and its value is approximately 0.3 m/s. Fig. 1 (b) shows the particle terminal velocity calculated for various equivalent diameters and sphericities of the particle.

As shown in Fig 1, it is hard to explain the collision between an actual bubble column and a particle column by comparing only the two terminal velocities. But by considering only the terminal velocity of a bubble (V_{TB}) moving inside a liquid and the terminal velocity of a particle (V_{TS}) under the same condition separately, a quantitative comparison between the terminal rising velocity of a bubble and the terminal velocity of a particle according to sphericity can be possible.

Fig. 2 shows the terminal velocity of a particle according to sphericity numerically, and the particle Reynolds number (Re_s) and drag coefficient obtained from the terminal velocity. In addition, compared to the terminal rising velocity of the bubble (~0.3 m/s) corresponding to the DAVINCI experiment conditions,

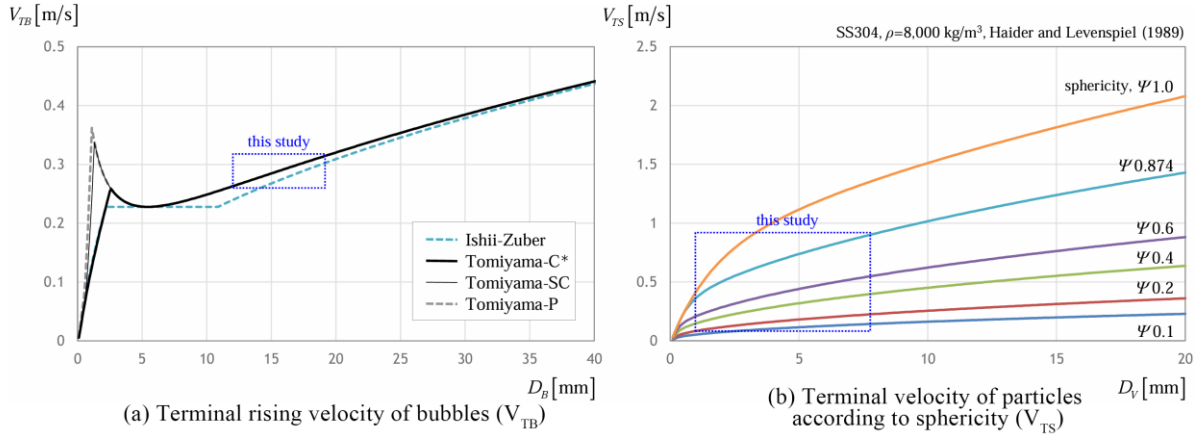


Fig. 1. Terminal velocity of bubble and particle.

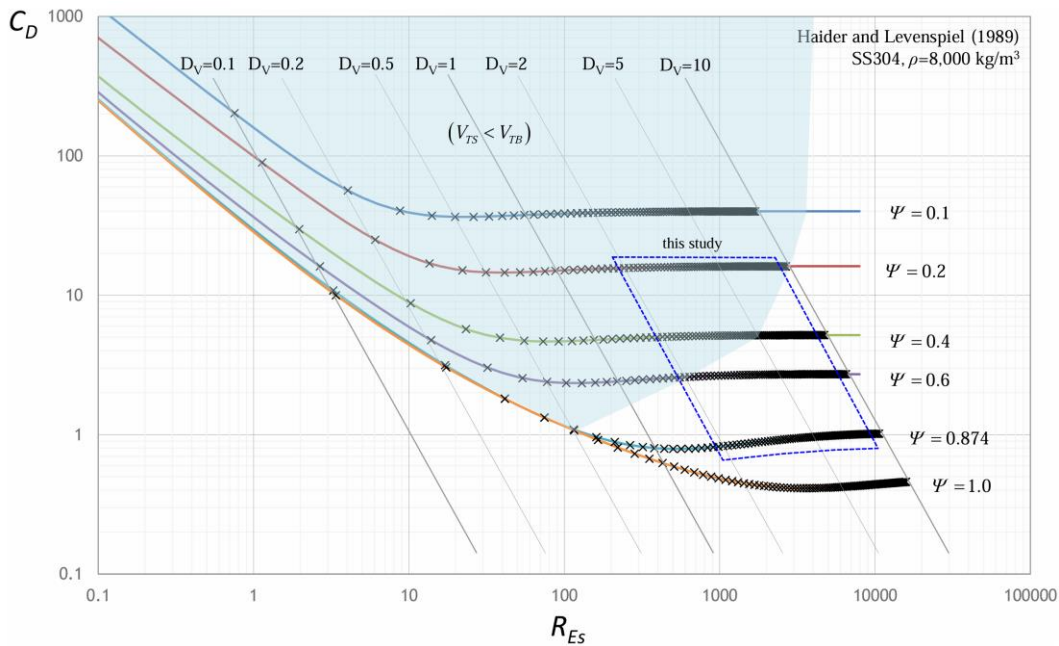


Fig. 2. Particle drag coefficient for particle size and sphericity.

the area where the terminal velocities of the particle (V_{TS}) are lower than the terminal rising velocity of the bubble (V_{TB}) is indicated as a shaded area. In case the terminal velocity of the particle (V_{TS}) is lower than the terminal rising velocity of the bubble (V_{TB}), it could be said that this is a condition in which the particle can easily change its falling trajectory due to the influence of the bubble behavior. Therefore, when the particle diameter is large and the sphericity is close to 1, it is less influenced by the bubble behavior. However, the particle with a high drag coefficient is more sensitive to the bubble behavior. The critical point seems to be roughly the terminal rising velocity of the bubble.

As indicated by the separate dotted line area in Fig. 2, this study attempted simulation by expanding the sphericity to 0.6, 0.4, 0.3, and 0.2 based on the previous result (sphericity 0.87) of Part I of the same-titled paper. The air flow rate for creating bubbles is indicated by Q_B , and four stages of 0 lpm, 30 lpm, 50 lpm, and 70 lpm were used. D_V means equivalent diameter, which is the

diameter of a perfect sphere with the same volume as the particle. All simulation conditions are the same as the DAVINCI experiment. For more details on the experiment and simulation, refer to Part I of the same-titled paper.

5. Results

A total of 80 simulations were performed with four levels of air flow rate conditions, five sphericity conditions, and four types of particle drops (except for the case of $D_V 0.92$) identical to those performed in the DAVINCI SG experiment, and the mass of particles collected in the particle catcher was investigated in the radial direction.

Fig. 3 shows the results of particles settled on the bottom when $D_V 1.95$ particles were released under the conditions of $Q_B 30$, $Q_B 50$, and $Q_B 70$ for five sphericities. Fig. 4 shows the mass distribution of particles settled on the bottom when $D_V 1.95$ particles

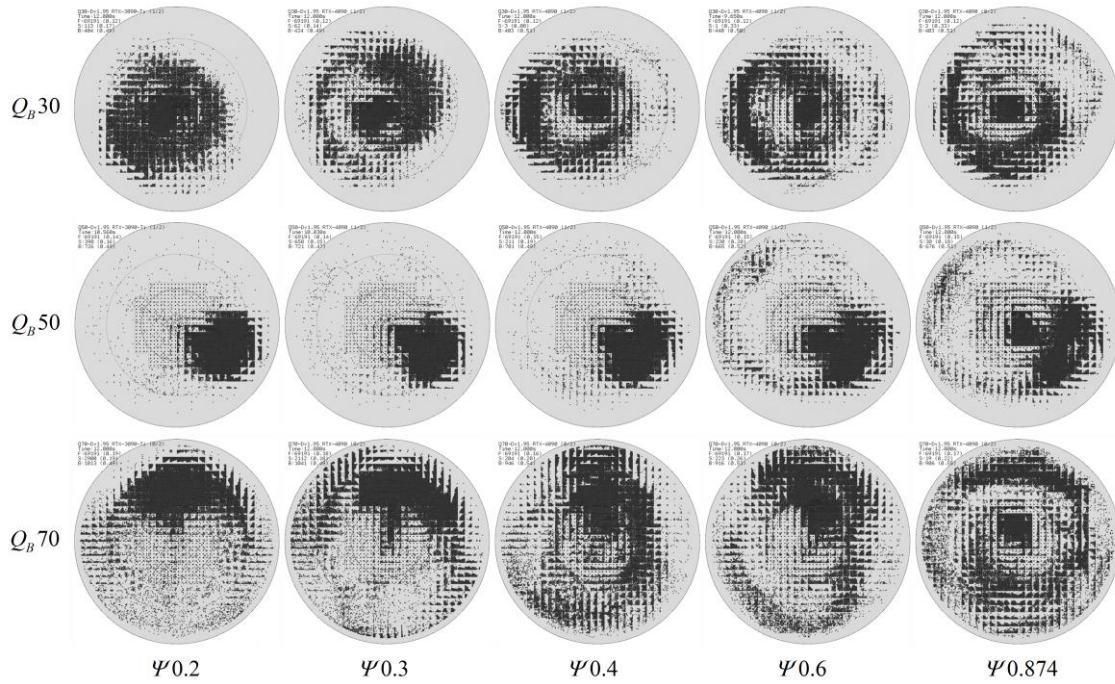


Fig. 3. Settled particles according to sphericity and air flow rate. (SG Dv1.95)

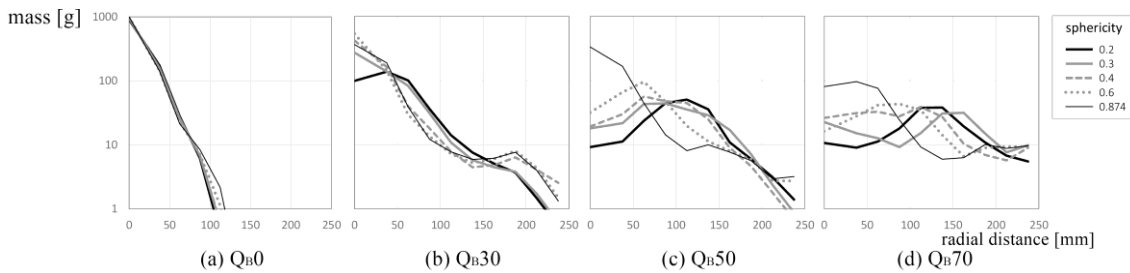


Fig. 4. Mass of settled particles in radial distance. (SG Dv1.95)

were released under the conditions of Q_{B30} , Q_{B50} , and Q_{B70} for five sphericities.

When a particle enters the water, it falls to the center and meets the center of the bubble column. However, if the air flow rate is sufficiently high or the particle diameter is small and the drag coefficient is high, the particle column begins to be disturbed, causing its trajectory to change in a random radial direction. The reason why the maximum mass distribution is measured at a specific radial position in Fig. 4 (c) and (d) is due to the reason explained above. These distributions mentioned above were observed in many cases except for $D_{v8.01}$ among the simulation conditions in this study.

Fig. 5 to 10 show the simulation results for different sized particles under five sphericities and four air flow rate conditions, similar to the above. Generally, the larger the particle size and the higher the sphericity, the less sensitive to the bubble's influence, and the particles tend to sediment the center of the bottom. As mentioned in Fig. 1 and 2 of Ch. 4, when V_{TS} is lower than V_{TB} , the bubble-induced effect becomes greater, and the particles are strongly scattered on the bottom.

According to sphericity, the 20 simulations were performed identically to the DAVINCI MT2 experiment for the particles mixed with five types in a certain ratio, and the results are shown in Fig. 11 to 14. Fig. 13 compares the composition ratio of particles captured in the central 40x40 mm area obtained by changing the air flow rate Q_B , and Fig. 14 compares the composition ratio of particles captured in the central area according to sphericity.

Although several correlations have been developed to evaluate the drag in monodisperse systems based on experimental data or numerical studies, it has been argued that when particles of different sizes are mixed (bidisperse or polydisperse system), to obtain the drag of a particle, not only the particle diameter, slip velocity, and local porosity but also the mean diameter of the surrounding particles should be considered. [6] It is known that the difference between monodisperse and bidisperse or polydisperse systems increases as the difference between the particle diameter and the mean diameter of the surrounding particles increases and the Reynolds number decreases.

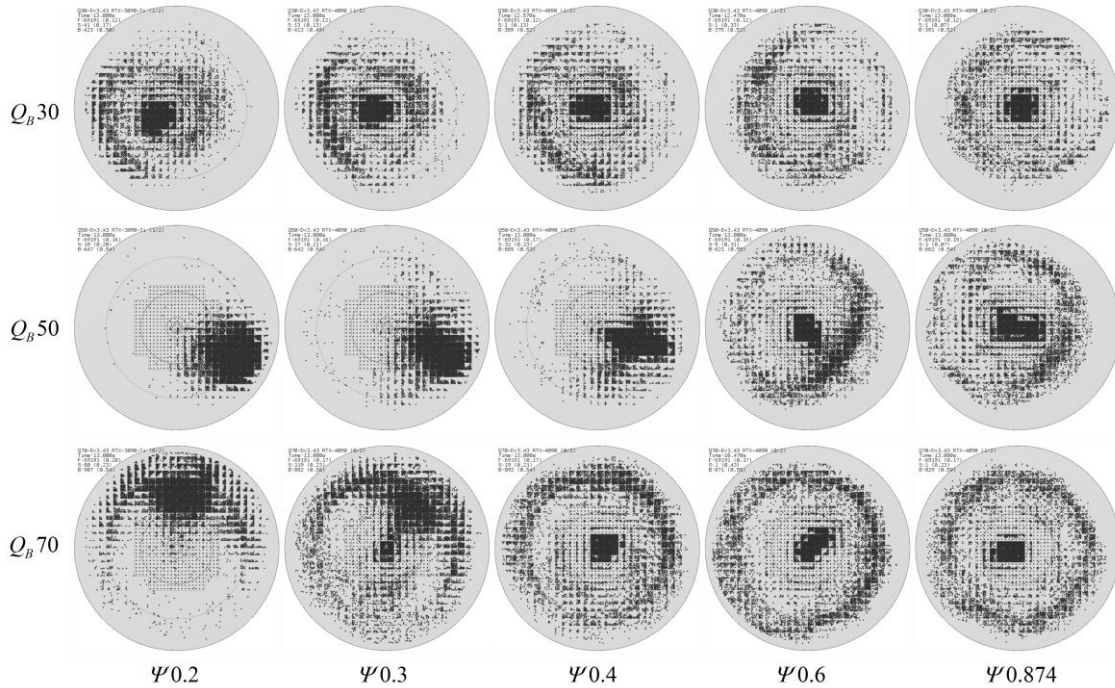


Fig. 5. Settled particles according to sphericity and air flow rate. (SG Dv3.43)

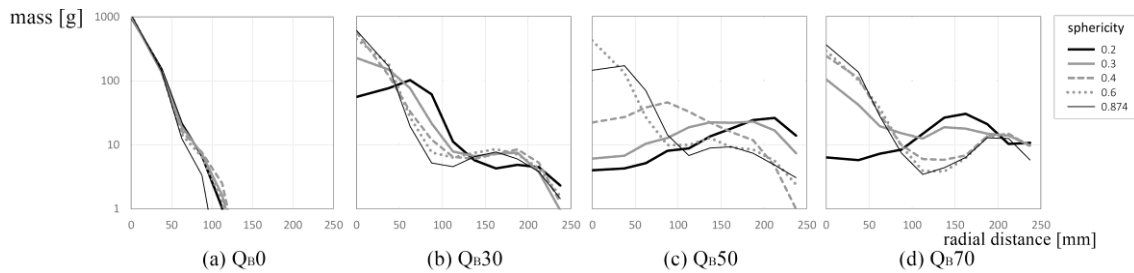


Fig. 6. Mass of settled particles in radial distance. (SG Dv3.43)

In this study, the MT2 simulations were performed using the conventional method excluding the effect of the mean diameter of the surrounding particles. This approach is usually called the *ad hoc* method. As shown in Figure 2, since the particle Reynolds number (Re_s) targeted in this study exceeds over 100, the difference is expected not to be significant.

Fig. 13 (a) shows the results obtained by changing the sphericity when particles are dropped without a bubble column, but it is difficult to say that a significant difference was observed. This is because the time allowed for particle settling is too short for the effect according to sphericity to reflect the influence of particle-induced turbulence. Comparing Fig. 13 (a) to (d), when bubbles are generated by air injection, their effect is very significant on the dispersion of particles.

Under the simulation conditions used in this study, a certain trend is observed in the results obtained according to sphericity and air flow rate. This could be explained by comparing the terminal velocity of a particle and the terminal rising velocity of a bubble as shown in Fig.1 and Fig.2.

6. Conclusions

In an unresolved method, we coupled MPS, DEM, and DBM using a fully Lagrangian approach to simulate the collision of the bubble column generated by air injection with the particle column formed by falling debris particles. Since our simulation results were quantitatively compared with the DAVINCI experiment in Part I of the paper of the same title, we investigated the mass distribution of particles settling on the bottom while changing the sphericity of the particles under the same conditions in this study.

Generally, the larger the particle size and the higher the sphericity, the less sensitive to the bubble's influence, and the particles tend to sediment the center of the bottom. The bubble-induced effect becomes stronger when the particle terminal velocity is lower than the terminal rising velocity of the bubble, which is determined from the influence of the drag coefficient and the particle size and sphericity, and the particles are strongly scattered on the bottom.

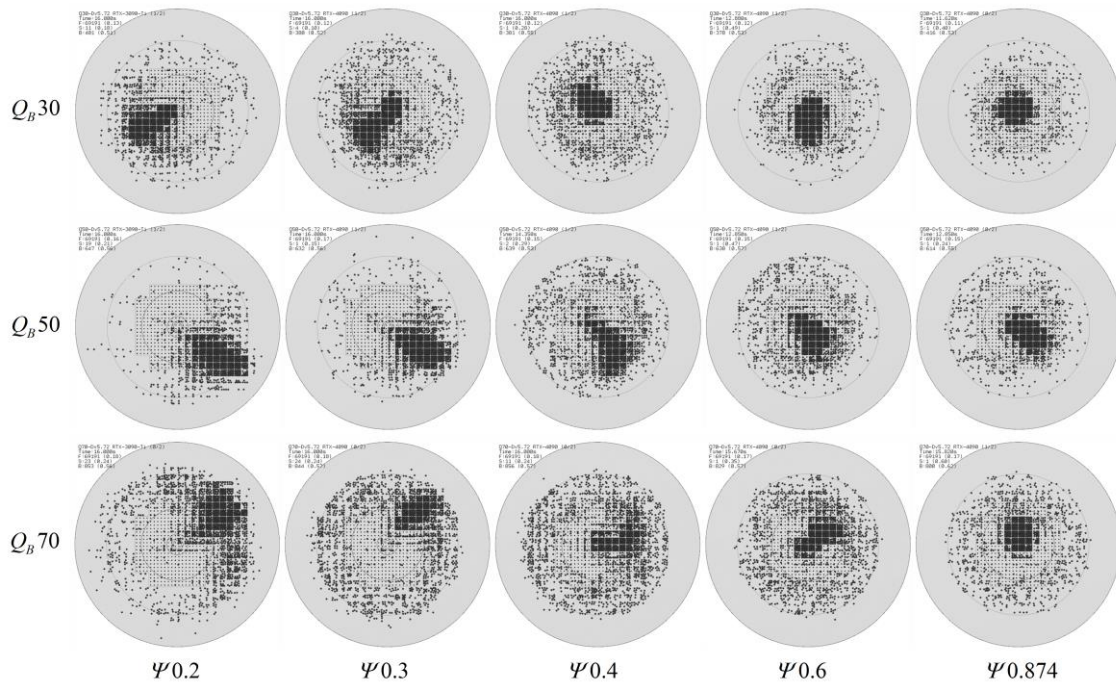


Fig. 7. Settled particles according to sphericity and air flow rate. (SG Dv5.72)

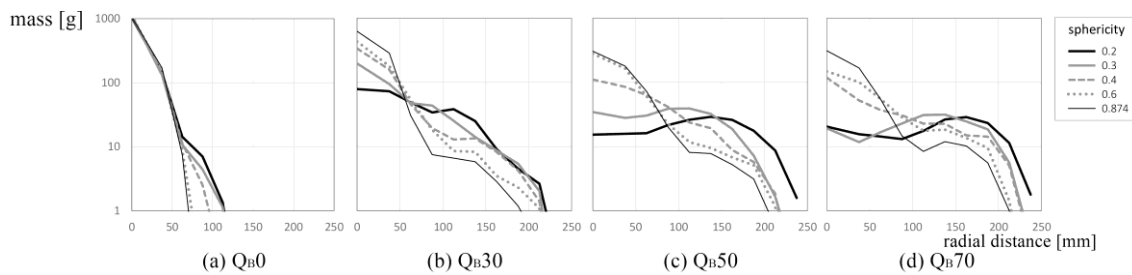


Fig. 8. Mass of settled particles in radial distance. (SG Dv5.72)

Even though the experiment was conducted under strictly controlled conditions and environments, the results of this experiment are expected to have some uncertainty.

According to Kim et al. [2], the bubbles measured at the center of the bubble column were non-spherical shapes (flattened ellipsoid), and under these conditions, a single bubble's rising trajectory instability occurs. It is known that the causes are the effects of the continuous shape instability of the bubble, the effects of the wake caused by the rising of the bubble, and the effects of contaminants contained in the liquid on the bubble surface. This is distinguished separately from the lift caused by the velocity gradient. Due to this rising trajectory instability, the bubble's path becomes uncertain, which affects the flow field and ultimately causes uncertainty in the falling trajectory of the falling particle.

The following limitations are pointed out in the numerical analysis.

First, the coalescence and breakup of bubbles were not considered in this study. When a rising bubble and a falling particle collide, it is expected that a large bubble

will be separated into many small bubbles, and it is expected that two rising bubbles will be regenerated into one bubble if certain conditions are met. However, research on this phenomenon is not yet sufficient, and although some researchers have attempted numerical analysis approaches, it seems that a clear model has not yet been established.

Second, the drag and lift forces calculated in dispersed phases such as bubbles and particles are steady forces, and unsteady forces are not considered. Research on this unsteady force is also insufficient, and it is pointed out that it has not been established yet, or numerical implementation requires a huge amount of memory and calculation. [8]

Third, the correlation used to obtain the lift force of particles is for spherical particles, and sphericity for expressing non-spherical particles is not considered.

Fourth, the turbulent Schmidt number used in calculating the turbulent dispersion of the dispersed phase is not a property of the liquid and is dependent on the state, so it is difficult to determine an appropriate constant value. This value can only be estimated as an appropriate value through experiments.

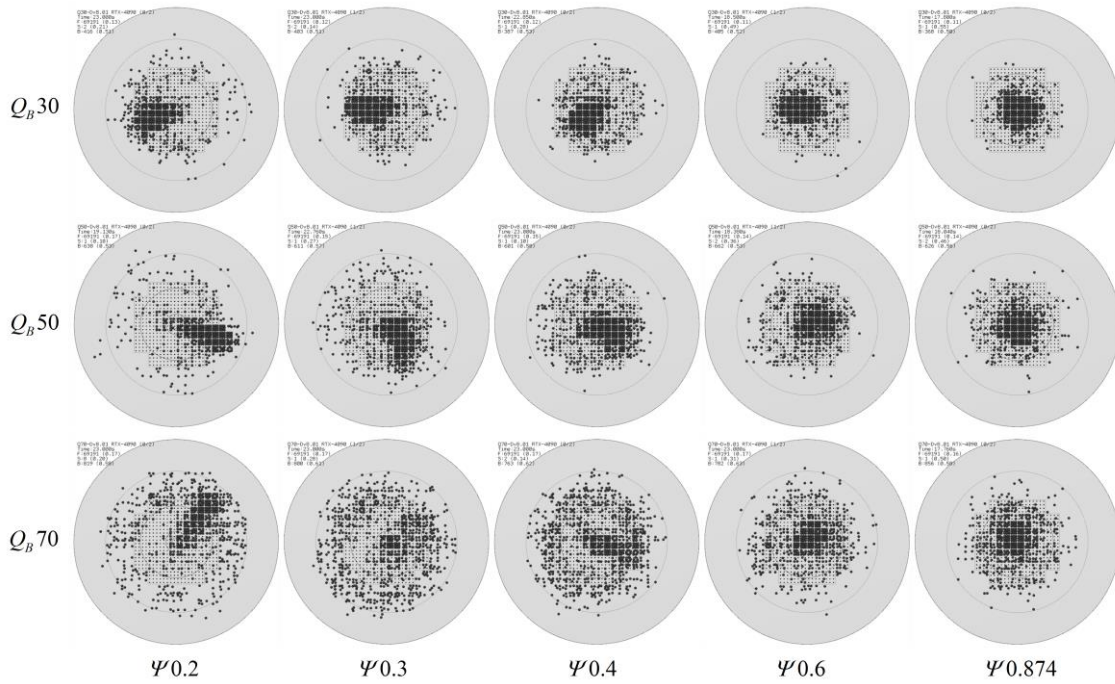


Fig. 9. Settled particles according to sphericity and air flow rate. (SG Dv8.01)

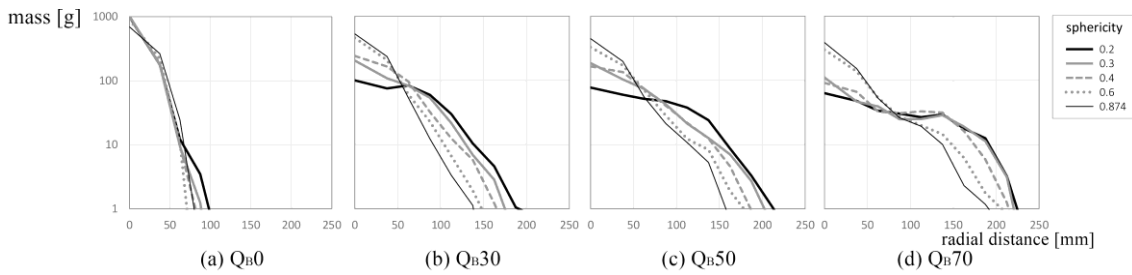


Fig. 10. Mass of settled particles in radial distance. (SG Dv8.01)

The results should be understood by considering the uncertainties of the phenomenon and the limitations of the numerical analysis mentioned above.

REFERENCES

- [1] E. Kim, W. Jung, J. Park, H. Park, and K. Moriyama, Experiments on Sedimentation of Particles in a Water Pool with Gas Inflow, *Nuclear Eng. and Tech.*, Vol. 48, pp. 457-469, 2016.
- [2] E. Kim, Debris Bed Formation during Ex-Vessel Severe Accidents in Light Water Reactors, Doctoral Thesis, Pohang University of Science and Technology, 2016.
- [3] Y. Jo, S. Park, H. Yoo, and E. Kim, GPU-based SPH-DEM Method to Examine the Three-Phase Hydrodynamic Interactions between Multiphase Flow and Solid Particles, *Int. J. of Multiphase Flow*, Vol. 153, 2022.
- [4] S. Koshizuka, K. Shibata, M. Kondo, and T. Matsunaga, *Moving Particle Semi-Implicit Method*, Academic Press, 2018.
- [5] E. Delnoij, J.A.M. Kuipers, and W. Van Swaaij, A three-dimensional CFD model for gas-liquid bubble columns. *Chem. Eng. Sci.*, Vol. 54, pp. 2217-2226, 1999.
- [6] H. Norouzi, R. Zarghami, R. Sotudeh-Gharebagh, and N. Mostoufi, *Coupled CFD-DEM Modeling: Formulation, Implementation and Application to Multiphase Flows*, Wiley, 2016.

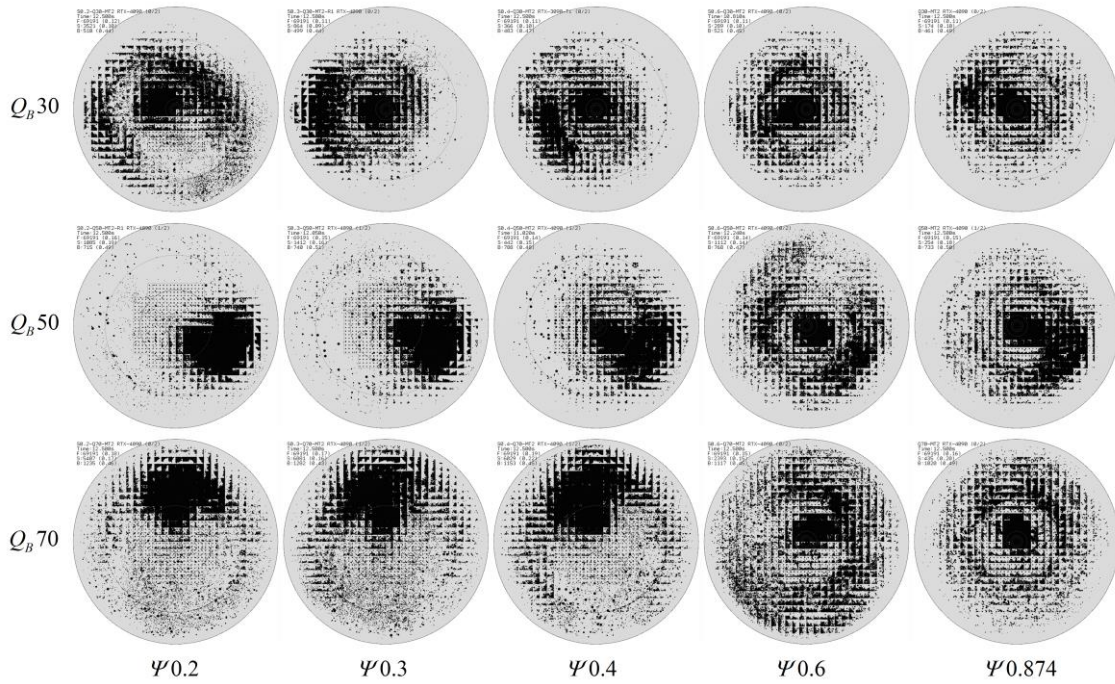


Fig. 11. Settled particles according to sphericity and air flow rate. (MT2)

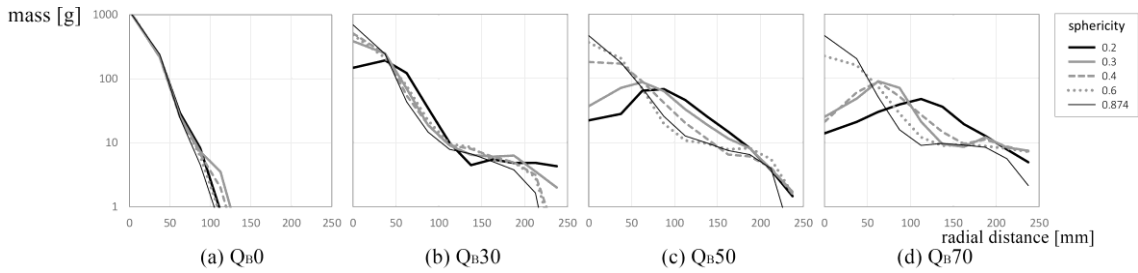


Fig. 12. Mass of settled particles in radial distance. (MT2)

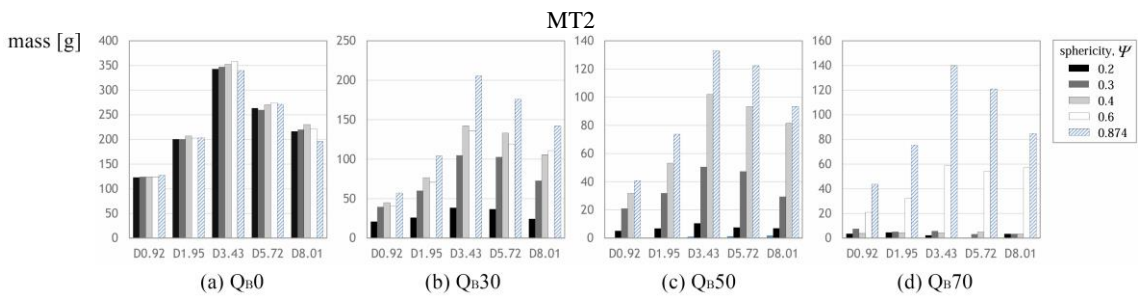


Fig. 13. Particle size distributions at the center region (40x40 mm) according to air flow rate. (MT2)

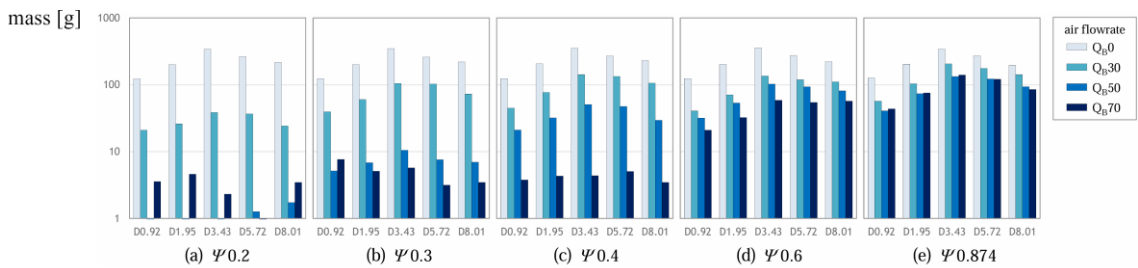


Fig. 14. Particle size distributions at the center region (40x40 mm) according to sphericity. (MT2)